HHS Public Access

Author manuscript

J Am Coll Cardiol. Author manuscript; available in PMC 2021 October 20.

Published in final edited form as:

J Am Coll Cardiol. 2020 October 20; 76(16): 1862–1874. doi:10.1016/j.jacc.2020.08.047.

Molecular Imaging of Apoptosis in Atherosclerosis by Targeting Cell Membrane Phospholipid Asymmetry

Farhan Chaudhry, MS[a,b,*], **Hideki Kawai, MD, PhD**[a,c,*], **Kipp W. Johnson, PhD**[a], **Navneet Narula, MD**[d], **Aditya Shekhar, BS**[a], **Fayzan Chaudhry, BS**[a], **Takehiro Nakahara, MD, PhD**[a], **Takashi Tanimoto, MD, PhD**[a], **Dongbin Kim, PhD**[a], **Matthew K.M.Y. Adapoe, MS**[a], **Francis G. Blankenberg, PhD**[e], **Jeffrey A. Mattis, PhD**[f], **Koon Y. Pak, PhD**[f], **Phillip D. Levy, MD, MPH**[b], **Yukio Ozaki, MD, PhD**[c], **Eloisa Arbustini, MD**[g], **H. William Strauss, MD**[a,h], **Artiom Petrov, PhD**[a], **Valentin Fuster, MD, PhD**[a,i], **Jagat Narula, MD, PhD**[a]

[a]Icahn School of Medicine at Mount Sinai, New York, New York

[b]Wayne State University School of Medicine, Detroit, Michigan

[c]Department of Cardiology, Fujita Health University, Toyoake, Aichi, Japan

[d]New York University Langone Medical Center, New York, New York

[e]Lucile Salter Packard Children's Hospital, Stanford, California

[f]Molecular Targeting Technologies, Inc., West Chester, Pennsylvania

[g]Policlinico San Matteo Pavia Fondazione IRCCS, Pavia, Italy

[h]Memorial Sloan Kettering Cancer Center, New York, New York

[i]Centro Nacional de Investigaciones Cardiovasculares Carlos III (CNIC), Madrid, Spain

Abstract

BACKGROUND—Apoptosis in atherosclerotic lesions contributes to plaque vulnerability by lipid core enlargement and fibrous cap attenuation. Apoptosis is associated with exteriorization of phosphatidylserine (PS) and phosphatidylethanolamine (PE) on the cell membrane. Although PS-avid radiolabeled annexin-V has been employed for molecular imaging of high-risk plaques, PE-targeted imaging in atherosclerosis has not been studied.

OBJECTIVES—This study sought to evaluate the feasibility of molecular imaging with PE-avid radiolabeled duramycin in experimental atherosclerotic lesions in a rabbit model and compare duramycin targeting with radiolabeled annexin-V.

METHODS—Of the 27 rabbits, 21 were fed high-cholesterol, high-fat diet for 16 weeks. Nine of the 21 rabbits received ^{99m}Tc-duramycin (test group), 6 received ^{99m}Tc-linear duramycin

ADDRESS FOR CORRESPONDENCE: Dr. Artiom Petrov, Mount Sinai Heart, One Gustave L. Levy Place, Guggenheim Pavilion West, 1190 Fifth Avenue, New York, New York 10029. artiom.petrov@mssm.edu.

*Drs. Chaudhry and Kawai contributed equally to the manuscript

The authors attest they are in compliance with human studies committees and animal welfare regulations of the authors' institutions and Food and Drug Administration guidelines, including patient consent where appropriate. For more information, visit the *JACC* author instructions page.

APPENDIX For supplemental videos, please see the online version of this paper.

(duramycin without PE-binding capability, negative radiotracer control group), and 6 received ^{99m}Tc-annexin-V for radionuclide imaging. The remaining normal chow-fed 6 animals (disease control group) received ^{99m}Tc-duramycin. In vivo microSPECT/microCT imaging was performed, and the aortas were explanted for ex vivo imaging and for histological characterization of atherosclerosis.

RESULTS—A significantly higher duramycin uptake was observed in the test group compared with that of disease control and negative radiotracer control animals; duramycin uptake was also significantly higher than the annexin-V uptake. Quantitative duramycin uptake, represented as the square root of percent injected dose per cm (√ID/cm) of abdominal aorta was >2-fold higher in atherosclerotic lesions in test group (0.08 ± 0.01%) than in comparable regions of disease control animals (0.039 ± 0.0061%, $p = 3.70 \cdot 10^{-8}$). Mean annexin uptake (0.060 ± 0.010%) was significantly lower than duramycin ($p = 0.001$). Duramycin uptake corresponded to the lesion severity and macrophage burden. The radiation burden to the kidneys was substantially lower with duramycin (0.49% ID/g) than annexin (5.48% ID/g; $p = 4.00 \cdot 10^{-4}$).

CONCLUSIONS—Radiolabeled duramycin localizes in lipid-rich areas with high concentration of apoptotic macrophages in the experimental atherosclerosis model. Duramycin uptake in atherosclerotic lesions was significantly greater than annexin-V uptake and produced significantly lower radiation burden to nontarget organs.

Keywords

annexin-V; cell death; duramycin; radionuclide imaging; vulnerable plaques

Numerous autopsy studies have demonstrated that histopathological composition of atherosclerotic lesions is associated with major adverse cardiac events (1,2). These features have been clinically identified by invasive intravascular ultrasound (IVUS), optical coherence tomography (OCT), and near infrared spectroscopy (NIRS) or noninvasive computed tomography angiography (CTA) imaging. Such compositional characteristics have been referred to as high-risk plaque (HRP) features and portend future events (3–6). CTA allows for the assessment of lipid rich, low-attenuation necrotic cores with positive vessel remodeling as the features of HRP (5). IVUS defines HRP as large necrotic cores abutting lumen, positive vessel remodeling, and minimal lumen area (3). OCT identifies thin-cap fibroatheroma (TCFA) and NIRS the extent of lipid burden (3,6). The absence of HRP features predicts relatively favorable outcomes (7). However, even though the presence of HRP features is associated with adverse events up to 10-year follow-up, plaque progression on serial CTA determines much higher likelihood of events (8). The extent of plaque inflammation is also suggested as an important determinant of plaque vulnerability (9). The inflammatory activity has been assessed at the systemic level by circulating biomarkers (such as high-sensitivity C-reactive protein [hsCRP]) and at the plaque level by altered perivascular fat attenuation on CTA, or targeted molecular imaging with radiotracers such as 18F-labeled fluorodeoxyglucose (FDG) and ^{99m}Tc-labeled annexin-V (10–14). Whereas the FDG uptake in atherosclerotic plaques is closely correlated to the extent of macrophage infiltration, annexin-V delineates the macrophages undergoing apoptosis and the magnitude of necrotic core (12,15).

Annexin-V binds avidly to phosphatidylserine (PS), which is exteriorized on the cell membrane following apoptosis (12,16). Inflammatory cell apoptosis leads to necrotic core enlargement, which constitutes the basis of plaque progression and fibrous cap attenuation (17). Although the PS-based molecular imaging has been used successfully both experimentally and clinically, it is associated with substantial radiation burden to nontarget organs. It is feasible to target yet another exteriorized phospholipid-phosphatidylethanolamine (PE) (18). PE is expressed more extensively in apoptotic cells and can be targeted by radiolabeled duramycin for molecular imaging with single-photon emission computed tomography (SPECT) imaging (19,20). Duramycin is an antibiotic with specific binding capabilities to PE. Because duramycin is a smaller molecule and can bind to the more abundant PE, radiolabeled duramycin has been shown to have lower nonspecific uptake, lower nontarget organ radiation burden, and better target-to-background ratio compared with annexin imaging (19,20) (Central Illustration).

In this study, we used ^{99m}Tc-labeled duramycin for the assessment of apoptosis in atherosclerotic lesions in an experimental rabbit model. Duramycin uptake was compared with radiolabeled annexin-V uptake through in vivo micro single-photon emission tomography-micro computed tomography (μSPECT-μCT) imaging, ex vivo imaging, and quantitative assessment of tracer uptake in the atherosclerotic lesions of varying severity. Radiotracer uptake was correlated with histopathological characterization of atherosclerotic lesions and the extent of plaque inflammation.

METHODS

THE EXPERIMENTAL PROTOCOL.

Animals.—Twenty-seven male New Zealand white rabbits, weighing 2.5 to 3.0 kg, were obtained from Charles River Breeding Laboratories Inc. (Wilmington, Massachusetts). Animals were housed according to National Institute of Health (NIH) guidelines, for an experimental protocol approved by the Laboratory Animal Care and Use Committee at the Icahn School of Medicine at Mount Sinai. After 2 weeks of quarantine, 21 rabbits were fed 0.3% cholesterol diet custom mixed in 6% peanut oil. One week after initiation of the high-cholesterol, high-fat diet, balloon de-endothelialization of the abdominal aorta was performed for induction of atherosclerotic lesions; the custom diet was then continued for 15 more weeks. The remaining 6 animals were fed normal rabbit chow and were left unmanipulated for the entire duration of the experiment (disease control group). Of the 21 experimental atherosclerotic animals, 9 received ^{99m}Tc-duramycin (test group), 6 received ^{99m}Tc-linear duramycin (duramycin without binding affinity to PE, negative radiotracer control), and 6 rabbits received ^{99m}Tc-annexin-V (positive radiotracer control group) for comparison with duramycin-based targeting. The 6 disease control animals received test tracer ^{99m}Tc-duramycin, for radionuclide imaging (Figure 1).

BALLOON DE-ENDOTHELIALIZATION PROCEDURE.

Twenty-one animals were anesthetized with a cocktail of ketamine and xylazine (100 mg/ml, 10:1 vol/vol; 1.5 to 2.5 ml subcutaneously). The right femoral artery was surgically exposed, a small arteriotomy site was created, and then 4F Fogarty embolectomy catheter (12–040-4F,

Edwards Life-sciences, Irvine, California) was advanced into the abdominal aorta under fluoroscopic guidance up to the aortic hiatus of the diaphragm. The catheter was then inflated and pulled back to the iliac bifurcation. After 5 passes, the catheter was removed, and the surgical cut-down site was closed with a 3–0 biodegradable suture. High-cholesterol, high-fat diet was fed to these animals 1 week before and 15 weeks after balloon de-endothelialization.

^{99m}Tc RADIOLABELING OF MOLECULAR TRACERS.

Hydrazinonicotinic acid (HYNIC)-duramycin and HYNIC-linear duramycin kits were obtained under a collaborative research agreement (Molecular Targeting Technologies, Inc., West Chester, Pennsylvania). Briefly, duramycin was covalently modified with succinimidyl 6-hydrazinonicotinate acetone hydrazone (S-HYNIC) at the distal end from the PE-binding pocket. The negative radiotracer control peptide—the linear duramycin (BAChem, Torrance, California) with a sequence (ARQAAAFGPFAFVADGNAR)—was used as a negative radiotracer control peptide. The linear duramycin has the same sequence as duramycin except that lysine amino acids at positions 2 and 19 are substituted with arginine, and the thioether-linked amino acids are replaced by alanine. It was also modified with S-HYNIC in a similar fashion as duramycin. The molecular weights (MWs) of the HYNIC-duramycin (expected MW = 2,188.4 g/mole, actual MW = 2,188.0 g/mole) and HYNIC-linear-duramycin (expected MW = 2,112.0 g/mole, actual MW = 2,112.0 g/mole) were confirmed using mass spectroscopy. Thereafter, ~30 mCi of ^{99m}Tc-pertechnetate in 0.5 ml of saline was added to the vial, and the excess vial pressure was vented. The vial was heated at 80°C (176°F) in a lead-lined heating block for 30 min. The radiolabel incorporation was assessed by radio-high-performance liquid chromatography analysis.

Human annexin-V was produced with *Escherichia coli* and labeled with ^{99m}Tc, as described previously (21), to be used as a positive control radiotracer.

RADIONUCLIDE IMAGING OF EXPERIMENTAL ATHEROSCLEROSIS.

Approximately 7 mCi of ^{99m}Tc-duramycin, ^{99m}Tc-annexin-V, or ^{99m}Tc-linear duramycin were administered intravenously. Using a dual-head μSPECT γ-camera equipped with μCT (Triumph SPECT-CT, Trifoil Imaging, Inc., Northridge, California), images of the thorax and abdomen were obtained immediately after radiotracer administration and 4 h later. Before imaging at 4 h, blood was obtained via ear vein to determine blood radiotracer level, measured as percent-injected dose per gram (%ID/g). In vivo SPECT images were acquired at 32 steps/detector (60 s per step) at the 140-keV photopeak of ^{99m}Tc, with 20% windows using low-energy, high-resolution parallel-hole collimator. The images were taken in 80 × 80 matrix format. After acquisition of μSPECT, a μCT scan was acquired, without moving the animal. The μCT was reconstructed from 512 views in 360° rotation with the x-ray tube operating at 80kVp and 500 μA. The μSPECT and μCT images were fused, allowing scintigraphic and anatomic information to be combined in the axial, sagittal, and coronal views as well as maximum intensity projection images. After obtaining the images, the rabbits were sacrificed with an overdose of pentobarbital sodium and phenytoin sodium solution through intravenous injection.

EX VIVO ASSESSMENT OF TRACER UPTAKE IN TARGET AND NONTARGET ORGANS.

The aortas were harvested and rinsed in saline. The ex vivo aortas were imaged for 1,800 s in the anterior and posterior projections with the high-resolution parallel-hole collimators. At the conclusion of ex vivo imaging, the aorta was measured and cut into 1-cm segments. Each segment was weighed and counted in an automatic well-type gamma-counter (PerkinElmer Wallac Inc., Gaithersburg, Maryland) for calculation of %ID/cm of the aorta. Livers, kidney cortices and medullas, and urine samples were extracted after sacrifice. Organs were weighted and gamma-counted to determine uptake of radiotracer (expressed as %ID/g).

PATHOLOGICAL CHARACTERIZATION OF AORTAS.

Preparation of aortic samples.—The aortic segments were fixed with 4-(2-hydroxyethyl)-1-piperazineethanesulfonic acid (HEPES)-buffered formalin (4%), containing an additional 2 mM of Ca^{2+}. In total, 84 specimens from 14 rabbits with experimental atherosclerosis and 24 specimens from 4 normal rabbits were histologically and immunohistochemically analyzed. Each specimen was subdivided into 3 equidistant sections and embedded on edge in paraffin. Serial 4-μm-thick sections were cut and mounted on charged slides (Superfrost, ThermoFisher Scientific, Waltham, Massachusetts). Tissue sections were stained with hematoxylin and eosin (H&E) and Movat Pentachrome (Abcam, Cambridge, United Kingdom) elastin staining.

DEFINITIONS OF ATHEROSCLEROTIC LESIONS.

Atherosclerotic lesions were defined as intimal xanthomas, early fibroatheromas, and late fibroatheromas (22). Intimal xanthomas were defined as plaques with superficial foam cell accumulation and no necrotic core, fibrous cap, or formation of thrombosis. Early fibroatheromas showed development of necrotic core and fibrous cap. Late fibroatheromas showed necrotic cores with the loss of cellular matrix and widespread cellular debris and distinct formation of fibrous cap. Both early and late fibroatheromas may have calcification.

HISTOLOGICAL ASSESSMENT OF EXPERIMENTAL ATHEROSCLEROSIS.

Pathological characterization of H&E and immunohistochemical-stained specimens was performed by 2 independent pathologists (N.N., E.A.). Immunohistochemical staining was undertaken for smooth-muscle actin and macrophages characterization on formalin-fixed paraffin-embedded tissue sections. The tissue sections were pre-treated using heat-mediated antigen retrieval with sodium citrate buffer (pH 6, epitope retrieval solution 1) for 30 min. The sections were then incubated with ENZ-30931 (ready-to-use) or M0633 (1:500 dilution) for 30 min at room temperature and detected using a horseradish peroxidase-conjugated compact polymer system; 3,3′-diaminobenzdine (DAB) was used as the chromogen. The sections were then counterstained with hematoxylin and mounted with Leica micro-mount (Leica Biosystems, Wetzlar, Germany).

A total area ranging from 3.8 to 4.1 mm^2 in 4 random high-power fields was counted in each of 28 randomly selected RAM-11 arterial sections from both duramycin and disease control animals. Aperio Image Scope (Leica Biosystems) analysis program was used with the

Positive Pixel Count v9 algorithm (Leica Biosystems) to count the immunohistochemical sections. The number of positive cells was divided by the total number of cells in that field to yield the positivity ratio: a method to assess relative macrophage activity in plaques (23). To correlate radiotracer uptake with histopathology, the positivity ratio for each cross-section was correlated with the cross-section's corresponding %ID/g radiotracer uptake.

STATISTICAL ANALYSES.

Sample size calculation was powered for detecting differences in radiotracer uptake to reach a beta-value of at least 0.80 with an alpha-value = 0.05 and a modest effect-size of 0.3 (G*Power 3.1 software was used). All results were expressed as mean ± SD. To determine the statistical significance of differences among groups, a 1-way analysis of variance (ANOVA) with a Tukey post hoc test was applied. Normality was assessed via Shapiro-Wilk's test. Variances and covariances were tested with Levene's test and Box's M test, respectively. For comparisons of radiotracer uptake of duramycin in the abdominal aorta compared with that seen in the thoracic aorta, a paired Student's *t*-test was performed. When testing for relationships between 2 nonparametric variables, a Spearman's rank-order correlation was used.

As there was significant difference in the weights of aortas among groups ($p = 1.1249 \cdot 10^{-7}$), the tracer concentration per cm of the aorta (%ID/cm) was calculated. Data were determined to be distributed normally when assessed via Shapiro-Wilk's test for normality ($p > 0.05$). Variances of %ID/cm were determined to be not homogenous ($p < 0.05$) when assessed with Levene's test for homogeneity of variances among groups. Therefore, for analysis, we transformed the ID/cm data by taking the square root of each value (√ID/cm), and variances were then determined to be homogenous ($p > 0.05$). There was homogeneity of covariances when assessed with Box's test of equality of covariance matrices ($p > 0.05$).

RESULTS

IN VIVO IMAGING.

The μSPECT-μCT in vivo images of radiolabeled duramycin for disease control and atherosclerotic animals are presented in Figure 2. Both groups of animals showed radiotracer in the blood pool of the aorta at 0 h. The disease control aortas in both sagittal and coronal views showed little uptake at 4 h. An intense uptake in both the coronal and sagittal views was observed at 4 h in the test-group animals. Fusion images showed aorta relative to the spine. Three-dimensional video visualization confirmed intense uptake of duramycin in atherosclerotic aortas (S1) compared with that from nonatherosclerotic aortas (S2). Blood %ID/g at 4 h was not significantly different among groups ($p = 0.0517$) (see below).

EX VIVO IMAGING.

The rabbit aorta SPECT ex vivo images are shown in Figure 3, with their corresponding gross pictures. There was comparatively similar uptake of radiolabeled duramycin (test radiotracer, Figure 3A) and annexin-V (positive control, Figure 3B), corresponding to regions with grossly visible atherosclerotic changes. There was minimal uptake of

radiolabeled linear duramycin (negative control, Figure 3C) in diseased animals, and minimal uptake of radiolabeled duramycin in disease control animals (Figure 3D).

QUANTITATIVE UPTAKE OF RADIOTRACERS IN AORTAS.

There was a significant difference in radiolabeled duramycin uptake among the groups in the abdominal aortic sections ($p = 1.69 \cdot 10^{-8}$). √ID/cm uptake of test tracer-duramycin (0.087 ± 0.01%, n = 9) was significantly higher in abdominal atherosclerotic lesions than that in the abdominal region of the unmanipulated animals (disease control group, 0.039 ± 0.0061%, n = 6, $p = 3.70 \cdot 10^{-8}$) and in abdominal atherosclerotic lesions after administration of radiolabeled linear duramycin (radiotracer negative control group; 0.045 ± 0.008%, $p = 6.11 \cdot 10^{-7}$). The calculated √ID/cm of duramycin showed a significantly greater uptake than annexin-V (positive radiotracer control group; 0.060 ± 0.010%, p = 0.001) in the abdominal sections. Duramycin uptake was significantly greater in abdominal sections than in thoracic sections of the same animal (0.0510 ± 0.00972 √ID/cm, $p = 4.00 \cdot 10^{-5}$). Uptake was not significantly different between the linear duramycin negative radiotracer control and the disease control ($p > 0.05$) groups.

QUANTITATIVE UPTAKE OF ^{99m}Tc-DURAMYCIN IN NONTARGET ORGANS.

The blood level of duramycin was 0.15 ± 0.05 %ID/g 4 h after injection; there was no significant difference in radiotracer's blood activity among groups. A 1-way ANOVA test was run to determine differences of nontarget organ uptake within groups. The differences among the tracers for liver, kidney cortex, and urine uptake were statistically significant ($p = 7.77 \cdot 10^{-8}$, $p = 5.20 \cdot 10^{-14}$, p = 0.024, respectively). Tukey post hoc tests in the diseased animals showed significantly greater uptake of annexin-V in the cortices of the kidney, compared with that seen from duramycin (5.48 ± 1.14 %ID/g vs. 0.4915 ± 0.116 %ID/g, $p = 9.95 \cdot 10^{-13}$) (Figure 4). Although outliers were detected by visual inspection by box plot, removing outliers did not change detection of statistical significance, and therefore outliers were kept in for analysis.

HISTOLOGICAL AND IMMUNOHISTOCHEMICAL CHARACTERISTICS OF ATHEROSCLEROSIS.

Figure 5A demonstrates the thoracic aorta of the animal injected with test radiotracer-duramycin. There is minimal intimal thickening as seen in the H&E staining, and RAM-11 staining shows macrophage accumulation along the wall. The actin staining shows smooth-muscle cell alignment in the tunica media. The uptake for this segment is 0.002269 %ID/cm. Figure 5B shows a section from the abdominal aorta of the same animal. The aorta on the H&E stain shows significant intimal thickening. On the RAM-11 staining, there is substantial macrophage accumulation along the intima. The radiotracer uptake is 0.006824 %ID/cm for this segment.

RAM-11 positivity ratio was determined to be non-normative ($p < 0.05$), and therefore a Spearman's rank-order correlation test was used to assess the relationship between radiotracer uptake and RAM-11 positivity ratio. The RAM-11 positivity ratio correlated with the respective piece-by-piece %ID/g ($r_s = 0.748$, $p = 2.00 \cdot 10^{-6}$) (Figure 5C). The caspase staining in the tissue sections was not attempted because, in the past, we have demonstrated

that the core macrophages closely correlate with the apoptosis radiotracers, and antibodies targeting activated-caspase 3 in rabbit atherosclerosis models are not readily available to evaluate apoptosis (24).

DISCUSSION

RADIOLABELED DURAMYCIN FOR IMAGING APOPTOSIS IN ATHEROSCLEROSIS.

The ability of radiolabeled annexin-V to image macrophage apoptosis has been demonstrated both clinically and in an experimental model of atherosclerosis (12,25). The current study was undertaken to determine differences in uptake of radiolabeled duramycin (that targets PE) compared with that seen with annexin-V (that targets PS) in the atherosclerotic lesions.

Duramycin binds to the head groups of PE with a high affinity at a 1:1 molar ratio (26). The expression of PE on the outer leaflet of the cell membrane in apoptotic cells occurs similarly as PS with the advantage that PE is more abundantly present. Once the cell membrane polarization is lost after the expression of scramblase, the increased concentration of PE offers more binding targets on apoptotic cells for PE-specific imaging agents (18). In addition, the structural attributes of duramycin make it a superior imaging agent, and its small molecular size, allows rapid diffusion to the extracellular spaces. Stabilized by 3 internal thioether linkages with no free peptidic termini, duramycin is resistant to in vivo proteolytic degradation. Presence of primary amines at the N-terminal offers convenient sites for covalent modification and radiolabeling, and the sites for molecular modification for radiolabeling are away from the PE-binding pocket at the distal end, thus providing minimal interference with the affinity of duramycin for PE binding (26). As demonstrated in our previous study of the experimental ischemia-reperfusion model, the ability of duramycin was similar to that seen from annexin-V for noninvasive imaging of apoptosis (19). However, in the current study, duramycin uptake was superior to annexin-V uptake for noninvasive imaging in atherosclerosis.

APOPTOSIS IN MACROPHAGES AND PLAQUE VULNERABILITY.

Macrophages within plaques are phenotypically heterogeneous and differentially contribute to development of plaque. However, it is believed that apoptosis and secondary necrosis of macrophages results information of necrotic core and could contribute to plaque rupture (27–29). In the study of culprit lesions obtained from victims of sudden coronary death, ruptured plaques and high-risk plaques showed extensive macrophage infiltration across the vessel wall and macrophage cell death via necrosis and apoptosis (17). Expansion of the necrotic core is likely the consequence of accelerated macrophage apoptosis and lack of efficient cell clearance (30). Abundance of cytokines among dying macrophages promotes matrix degradation and fibrous cap attenuation. Dying macrophages also serve as a nidus for microcalcification, which, when superficial, might contribute to susceptibility to plaque rupture (1). Furthermore, macrophage apoptosis may also facilitate the acute thrombotic event arising from the rupture itself. Elegant studies have captured the shed membrane microparticles originating from culprit plaques as the products of apoptotic cells; the

microparticles were primarily monocytic in origin and very rich in tissue factor and procoagulant activity (31,32).

IDENTIFICATION OF APOPTOTIC MACROPHAGES.

It can be theorized, therefore, that delineating the extent of these apoptotic macrophages could correlate with the extent of necrotic core and thus possibly HRP (27–29,33,34). Our findings correspond to a small previous experiment showing significantly greater duramycin uptake compared with annexin-V uptake in atherosclerotic aortas from ApoE−/− mice (n = 3) (35). The authors demonstrated significant correlation of duramycin uptake with apoptotic cells but did not correlate duramycin uptake with macrophage accumulation. Other cells, such as smooth-muscle cells and endothelial cells, undergo apoptosis during plaque formation; however, as mentioned before, macrophage apoptosis and subsequent mediator release is likely the main driving force behind necrotic core expansion.

We observed that duramycin uptake was focalized to areas of grossly visible plaque formation on ex vivo imaging and was visible in vivo, regardless of the presence of the kidneys on both sides of the aorta. Higher radiation burden to kidneys interferes in annexin-V imaging in similar circumstances. These findings suggest that duramycin uptake might play a role in delineation of HRP. As murine, rabbit, and primate atherosclerosis models do not mimic rupture seen clinically, serial images would therefore be required in humans to test whether accumulation of duramycin in atherosclerotic plaques would be of translational clinical value (36).

LOW NONTARGET UPTAKE OF RADIOLABELED DURAMYCIN.

Evaluation of chronic diseases with serial imaging requires minimal off-target radiation burden. Duramycin is a small molecule that showed less radiation burden to kidneys compared with the larger charged annexin-V (19). Having lower off-target radiation burden also prevents any potential interference from nonspecific signaling, thereby improving image quality. Overall, off-target radiation burden with duramycin and annexin-V was similar to our previous rabbit studying, indicating consistency of results (19).

As the molecular weight of annexin-V (36,000) is much different from duramycin, it could be questioned that the equal radioactivity dose of each chemical might not be comparable and that more molecules of smaller duramycin than annexin-V could explain the greater uptake. In fact, there are more sites for duramycin to bind in comparison with annexin-V. We did not normalize the 2 probes because of the following (37,38): the affinity of the annexin-V (3 nm) is 2 times higher than duramycin (6 nm); the effective dose of annexin-V 4-fold higher than duramycin (annexin-V 0.011 mSv/MBq, duramycin 0.003 msV/MBq); and annexin-V binds to a variety of lipids such as phosphatidylinositol and likely PE, in addition to PS, whereas duramycin only binds to PE.

CLINICAL PERSPECTIVES.

With the emerging data, it is becoming clear that the plaque progression due to expansion of necrotic core is the basis of future events (8,39). Regardless of the extent of luminal stenosis, the magnitude of necrotic core also determines the physiological behavior of the lesion and

influences the fractional flow reserve and the outcomes (40). The prospective observational component of an ongoing PROSPECT (Providing Regional Observations to Study Predictors of Events in the Coronary Tree)-II study using multimodality imaging is the examination of the natural history of atherosclerotic lesions in terms of their susceptibility to plaque rupture and clinical events (NCT02171065). Owing to lack of availability of precise measurements of the necrotic cores in HRP by the IVUS and CTA images, this study is using plaque burden ≥65% as the primary threshold defining vulnerable plaques; the sensitivity analyses will be run for lesions with ≥70% burden. Near-infrared spectroscopic imaging provides a quantitative assessment of lipid burden and is being used to accomplish the substudy of the PROSPECT-II Absorb, wherein the treatment of HRP with bioresorbable vascular scaffold will be compared with medical therapy alone at 25 months. It is expected that the molecular imaging of cell death could provide a reliable noninvasive estimate of necrotic core, similar to invasive lipid core burden index (41,42), and help to improve risk-stratification.

STUDY LIMITATIONS.

The histopathologic severity of the atherosclerotic lesions was correlated with the duramycin uptake in the current study, and the common apoptotic staining methods (such as terminal deoxynucleotidyl transferase dUTP nick end labeling [TUNEL] and active caspase staining) were not used. However, in previous studies, it has been extensively validated that duramycin is a specific marker for apoptosis (19,26,35). In the current study, we correlated the extent of macrophage infiltration with the duramycin uptake and reasonably assumed that duramycin targeted apoptotic cells in the atherosclerotic lesions. Furthermore, it is believed that the apoptosis of macrophages should enlarge the necrotic core size and add to the plaque vulnerability. Higher degree of macrophage infiltration and apoptosis has been demonstrated in carotid atherosclerosis in patients undergoing endarterectomy, but none of the clinical studies has prospectively demonstrated the importance of apoptosis as a prognostic marker (25). Furthermore, as mentioned before, the development of atherosclerosis in this experimental model, although similar in pathogenesis, is not exactly the same as seen in humans (36). Humans accumulate atherosclerosis over the course of years, whereas these experimental models are studied only over several weeks. Therefore, it would be of interest to perform serial duramycin studies clinically to address temporal development of necrotic core formation and its relation to adverse outcomes. Regardless, this model served its purpose, as we were able to show that radiolabeled duramycin localized to atherosclerotic lesions. Finally, it is important to note that current preclinical μSPECT machines have higher spatial resolution when compared with that seen for clinical SPECT equipment (43). Higher spatial resolution is crucial to mitigate partial volume loss and spillover effects when imaging small objects. Therefore, using PET-based imaging modalities can be argued to be more practical. ^{18}F-FDG-PET imaging has effectively monitored plaque inflammation and response to therapy in humans; however, owing to high nonspecific myocardial uptake and high operating costs, 18F-FDG imaging of coronary plaques is limited (44).

CONCLUSIONS

The current study demonstrates the feasibility of radiolabeled duramycin to identify apoptosis in atherosclerotic lesions. Radionuclide duramycin demonstrates greater uptake in atherosclerotic lesions compared with radiolabeled annexin-V imaging, while having significantly less radiation burden to nontarget organs. Targeted imaging with duramycin should contribute as an attractive strategy for the assessment of the magnitude of necrotic cores and potentially high-risk atherosclerotic plaques.

Supplementary Material

Refer to Web version on PubMed Central for supplementary material.

Acknowledgments

Part of the data was presented by Dr. Farhan Chaudhry at The Society of Nuclear Medicine and Molecular Imaging Mid-Winter Meeting and the American College of Nuclear Medicine Annual Meeting in January 2016 in Orlando, Florida, and won the Best Young Investigator Award. This manuscript is dedicated to the memory of Dr. Farooq A. Chaudhry (August 30, 2017), who initiated the project in collaboration with Drs. Narula and Fuster. Drs. Mattis and Pak are employees of Molecular Targeting Technologies, Inc. Funding support was received from NIH SBIR Contract Research grant (project # 268201400043C-0-0-1) to Dr. Narula. Dr. Chaudhry's research fellowship was partially funded by the Society of Academic Emergency Medicine Foundation and the Jewish Fund. All other authors have reported that they have no relationships relevant to the contents of this paper to disclose. Ahmed Tawakol, MD, served as Guest Associate Editor for this paper. Deepak L. Bhatt, MD, MPH, served as Guest Editor-in-Chief for this paper.

ABBREVIATIONS AND ACRONYMS

CTA	computed tomography angiography
FDG	18F-labeled fluorodeoxyglucose
HRP	high-risk plaque
ID	injected dose
IVUS	intravascular ultrasound
μCT	micro computed tomography
μSPECT	micro single-photon emission computed tomography
NIRS	near infrared spectroscopy
OCT	optical coherence tomography
PE	phosphatidylethanolamine
PS	phosphatidylserine
TCFA	thin-cap fibroatheroma

REFERENCES

1. Burke AP, Farb A, Malcom GT, Liang YH, Smialek J, Virmani R. Coronary risk factors and plaque morphology in men with coronary disease who died suddenly. N Engl J Med 1997;336: 1276–82. [PubMed: 9113930]
2. Narula J, Nakano M, Virmani R, et al. Histopathologic characteristics of atherosclerotic coronary disease and implications of the findings for the invasive and noninvasive detection of vulnerable plaques. J Am Coll Cardiol 2013;61:1041–51. [PubMed: 23473409]
3. Stone GW, Maehara A, Lansky AJ, et al. A prospective natural-history study of coronary atherosclerosis. N Engl J Med 2011;364:226–35. [PubMed: 21247313]
4. Jia H, Abtahian F, Aguirre AD, et al. In vivo diagnosis of plaque erosion and calcified nodule in patients with acute coronary syndrome by intravascular optical coherence tomography. J Am Coll Cardiol 2013;62:1748–58. [PubMed: 23810884]
5. Motoyama S, Kondo T, Sarai M, et al. Multislice computed tomographic characteristics of coronary Lesions in acute coronary syndromes. J Am Coll Cardiol 2007;50:319–26. [PubMed: 17659199]
6. Waksman R, Di Mario C, Torguson R, et al. Identification of patients and plaques vulnerable to future coronary events with near-infrared spectroscopy intravascular ultrasound imaging: a prospective, cohort study. Lancet 2019;394: 1629–37. [PubMed: 31570255]
7. Kaul S, Narula J. In search of the vulnerable plaque: is there any Light at the end of the catheter? J Am Coll Cardiol 2014;64:2519–24. [PubMed: 25500238]
8. Motoyama S, Ito H, Sarai M, et al. Plaque characterization by coronary computed tomography angiography and the likelihood of acute coronary events in mid-term follow-up. J Am Coll Cardiol 2015;66:337–46. [PubMed: 26205589]
9. Libby P Mechanisms of acute coronary syndromes and their implications for therapy. N EngL J Med 2013;368:2004–13. [PubMed: 23697515]
10. Ridker PM, Everett BM, Thuren T, et al. Anti-inflammatory therapy with canakinumab for atherosclerotic disease. N Engl J Med 2017;377: 1119–31. [PubMed: 28845751]
11. Oikonomou EK, Marwan M, Desai MY, Mancio J, Alashi A, Hutt Centeno E, et al. Non-invasive detection of coronary inflammation using computed tomography and prediction of residual cardiovascular risk (the CRISP CT study): a post-hoc analysis of prospective outcome data. Lancet 2018;392:929–39. [PubMed: 30170852]
12. Kolodgie FD, Petrov A, Virmani R, et al. Targeting of apoptotic macrophages and experimental atheroma with radiolabeled annexin V: a technique with potential for noninvasive imaging of vulnerable plaque. Circulation 2003;108: 3134–9. [PubMed: 14676140]
13. Rogers IS, Nasir K, Figueroa AL, et al. Feasibility of FDG imaging of the coronary arteries. J Am Coll Cardiol Img 2010;3:388–97.
14. Tahara N, Imaizumi T, Virmani R, Narula J. Clinical feasibility of molecular imaging of plaque inflammation in atherosclerosis. J Nucl Med 2009; 50:331–4. [PubMed: 19223412]
15. Tahara N, Mukherjee J, De Haas HJ, et al. 2-deoxy-2-[18F]fluoro-d-mannose positron emission tomography imaging in atherosclerosis. Nat Med 2014;20:215–9. [PubMed: 24412923]
16. Tanimoto T, Parseghian MH, Nakahara T, et al. Cardioprotective effects of HSP72 administration on ischemia-reperfusion injury. J Am Coll Cardiol 2017;70:1479–92. [PubMed: 28911512]
17. Kolodgie FD, Narula J, Burke AP, et al. Localization of apoptotic macrophages at the site of plaque rupture in sudden coronary death. Am J Pathol 2000;157:1259–68. [PubMed: 11021830]
18. Pomorski TG, Menon AK. Lipid somersaults: uncovering the mechanisms of protein-mediated lipid flipping. Prog Lipid Res 2016;64:69–84. [PubMed: 27528189]
19. Kawai H, Chaudhry F, Shekhar A, et al. Molecular imaging of apoptosis in ischemia reperfusion injury with radiolabeled duramycin targeting phosphatidylethanolamine: effective target uptake and reduced nontarget organ radiation burden. J Am Coll Cardiol Img 2018;11:1823–33.
20. Shekhar A, Heeger P, Reutelingsperger C, et al. Targeted imaging for cell death in cardiovascular disorders. J Am Coll Cardiol Img 2018;11: 476–93.

21. Blankenberg FG, Katsikis PD, Tait JF, et al. In vivo detection and imaging of phosphatidylserine expression during programmed cell death. Proc Natl Acad Sci 1998;95:6349–54. [PubMed: 9600968]
22. Yahagi K, Kolodgie FD, Otsuka F, et al. Pathophysiology of native coronary, vein graft, and instent atherosclerosis. Nat Rev Cardiol 2016;13: 79–98. [PubMed: 26503410]
23. Hsu S, Koren E, Chan Y, et al. Effects of everolimus on macrophage-derived foam cell behavior. Cardiovasc Revasc Med 2014;15:269–77. [PubMed: 24972512]
24. Fan J, Chen Y, Yan H, Niimi M, Wang Y, Liang J. Principles and applications of rabbit models for atherosclerosis research. J Atheroscler Thromb 2018;25:213–20. [PubMed: 29046488]
25. Kietselaer BLJH, Reutelingsperger CPM, Heidendal GAK, et al. Noninvasive detection of plaque instability with use of radiolabeLed annexin A5 in patients with carotid-artery atherosclerosis. N Engl J Med 2004;350:1472–3.
26. Audi S, Li Z, Capacete J, et al. Understanding the in vivo uptake kinetics of a phosphatidylethanolamine-binding agent 99mTc-duramycin. Nucl Med Biol 2012;39:821–5. [PubMed: 22534031]
27. Chaudhry F, Isherwood J, Bawa T, et al. Single-cell RNA sequencing of the cardiovascular system: new looks for old diseases. Front Cardiovasc Med 2019;6:173. [PubMed: 31921894]
28. Seimon T, Tabas I. Mechanisms and consequences of macrophage apoptosis in atherosclerosis. J Lipid Res 2009;50 Suppl:S382–7. [PubMed: 18953058]
29. Moore KJ, Sheedy FJ, Fisher EA. Macrophages in atherosclerosis: a dynamic balance. Nat Rev Immunol 2013;13:709–21. [PubMed: 23995626]
30. Garbin U, Baggio E, Stranieri C, et al. Expansion of necrotic core and shedding of Mertk receptor in human carotid plaques: a role for oxidized polyunsaturated fatty acids? Cardiovasc Res 2013;97:125–33. [PubMed: 22997156]
31. Mallat Z, Hugel B, Ohan J, Leseche G, Freyssinet JM, Tedgui A. Shed membrane microparticles with procoagulant potential in human atherosclerotic plaques: a role for apoptosis in plaque thrombogenicity. Circulation 1999;99:348–53. [PubMed: 9918520]
32. Laufer EM, Winkens MH, Narula J, Hofstra L. Molecular imaging of macrophage cell death for the assessment of plaque vulnerability. Arterioscler Thromb Vasc Biol 2009;29:1031–8. [PubMed: 19461053]
33. Martinez FO, Gordon S, Locati M, Mantovani A. Transcriptional profiling of the human monocyte-to-macrophage differentiation and polarization: new molecules and patterns of gene expression. J Immunol 2006;177:7303. [PubMed: 17082649]
34. Cochain C, Vafadarnejad E, Arampatzi P, et al. Single-cell RNA-Seq reveals the transcriptional landscape and heterogeneity of aortic macrophages in murine atherosclerosis. Circ Res 2018; 122:1661–74. [PubMed: 29545365]
35. Hu Y, Liu G, Zhang H, et al. A comparison of [99mTc] duramycin and [99mTc] annexin V in SPECT/CT imaging atherosclerotic plaques. Mol Imaging Biol 2018;20:249–59. [PubMed: 28785938]
36. Getz GS, Reardon CA. Animal models of atherosclerosis. Arterioscler Thromb Vasc Biol 2012;32:1104–15. [PubMed: 22383700]
37. Elvas F, Vangestel C, Pak K, Vermeulen P, Gray B, Stroobants S, et al. Early prediction of tumor response to treatment: preclinical validation of 99mTc-duramycin. J Nucl Med 2016;57: 805–11. [PubMed: 26837335]
38. Palmowski K, Rix A, Lederle W, Behrendt FF, Mottaghy FM, Gray BD, et al. A low molecular weight zinc2+-dipicolylamine-based probe detects apoptosis during tumour treatment better than an annexin V-based probe. Eur Radiol 2014; 24:363–70. [PubMed: 24121671]
39. Ahmadi A, Argulian E, Leipsic J, Newby DE, Narula J. From subclinical atherosclerosis to plaque progression and acute coronary events. J Am Coll Cardiol 2019;74:1608–17. [PubMed: 31537271]
40. Ahmadi A, Leipsic J, Ovrehus KA, et al. Lesion-specific and vessel-related determinants of fractional flow reserve beyond coronary artery stenosis. J Am Coll Cardiol Img 2018;11: 521–30.
41. Stone GW, Maehara A, Muller JE, et al., CANARY Investigators. Plaque characterization to inform the prediction and prevention of periprocedural myocardial infarction during percutaneous

coronary intervention: the CANARY trial (coronary assessment by near-infrared of atherosclerotic rupture-prone yellow). J Am Coll Cardiol Intv 2015;8:927–36.

42. Schuurman A-S, Vroegindewey M, Kardys I, et al. Near-infrared spectroscopy-derived lipid core burden index predicts adverse cardiovascular outcome in patients with coronary artery disease during long-term follow-up. Eur Heart J 2018;39: 295–302. [PubMed: 28531282]
43. Meester EJ, Krenning BJ, de Swart J, et al. Perspectives on small animal radionuclide imaging: considerations and advances in atherosclerosis. Front Med 2019;6:39.
44. Tawakol A, Fayad ZA, Mogg R, et al. Intensification of statin therapy results in a rapid reduction in atherosclerotic inflammation: results of a multicenter fluorodeoxyglucose-positron emission tomography/computed tomography feasibility study. J Am Coll Cardiol 2013;62:909–17. [PubMed: 23727083]

PERSPECTIVES

COMPETENCY IN MEDICAL KNOWLEDGE:

Apoptosis contributes to the progression of atherosclerotic plaques. Although ^{99m}Tc-annexin-V can be used for noninvasively imaging of apoptosis in atherosclerosis, the phosphatidylethanolamine-specific ^{99m}Tc-duramycin tracer provides better target uptake with less radiation to nontarget organs, potentially offering a more attractive approach to serial characterization of high-risk plaques.

TRANSLATIONAL OUTLOOK:

Clinical studies of molecular imaging of apoptosis in atherosclerotic lesions may offer insights into plaque progression and vulnerability.

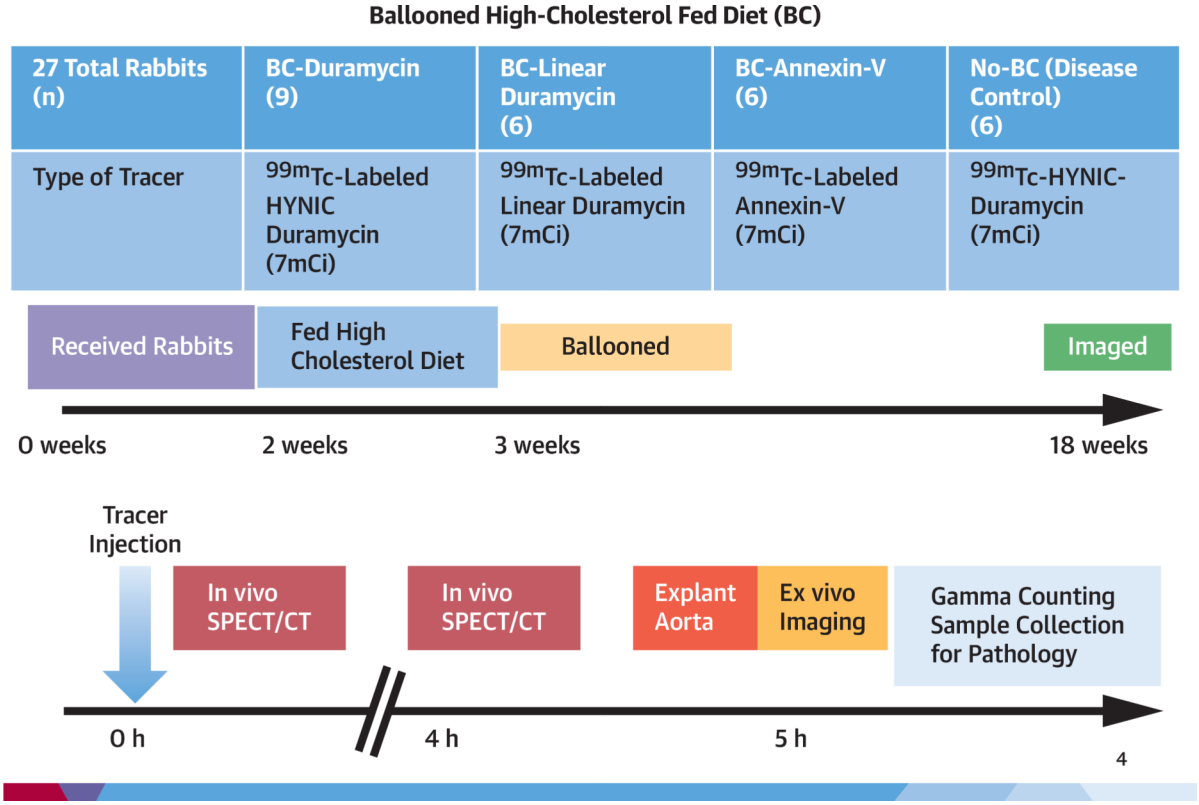

FIGURE 1. Experimental Protocol and Timeline

Various experimental groups and a timeline of experimental protocol.

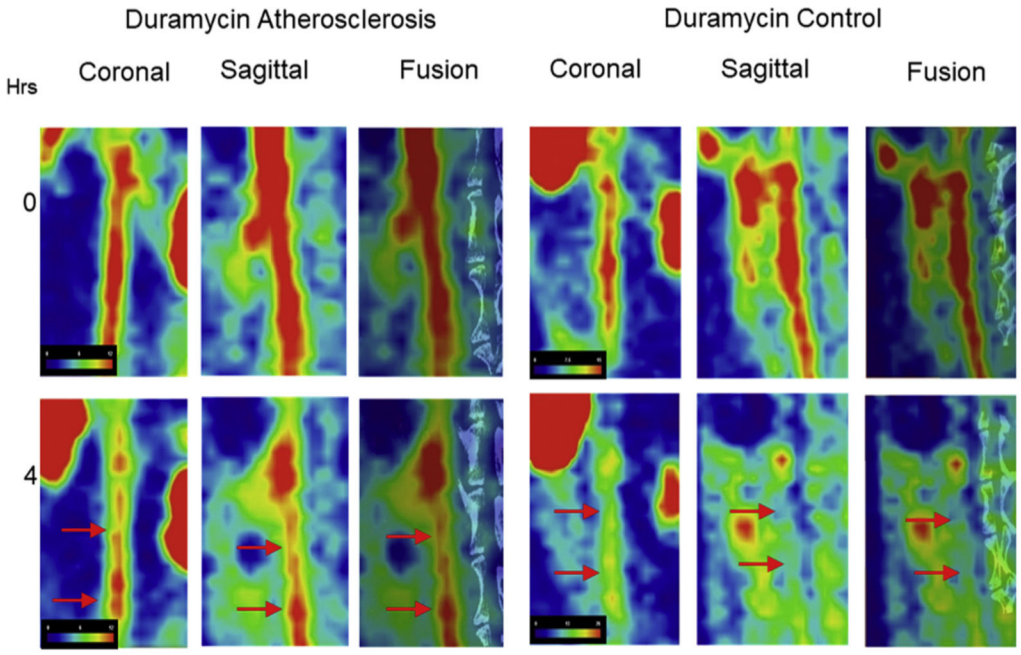

FIGURE 2. In Vivo Images of Atherosclerotic Lesions With Radiolabeled Duramycin

In vivo images of the abdominal aorta of the atherosclerotic animal **(left)** and the disease control animal **(right)** injected with 99mTc-duramycin (test tracer) at 0 **(top)** and 4 h **(bottom)**. Please note radiotracer uptake in the abdominal aorta of the atherosclerotic animal **(red arrows, left)** compared with the disease control animal **(red arrows, right)** at 4 h. Please refer to Video 1 for 3D video visualization of duramycin uptake at 4 h in abdominal aorta of atherosclerotic rabbit and Video 2 for lack of uptake in abdominal aorta of control animal.

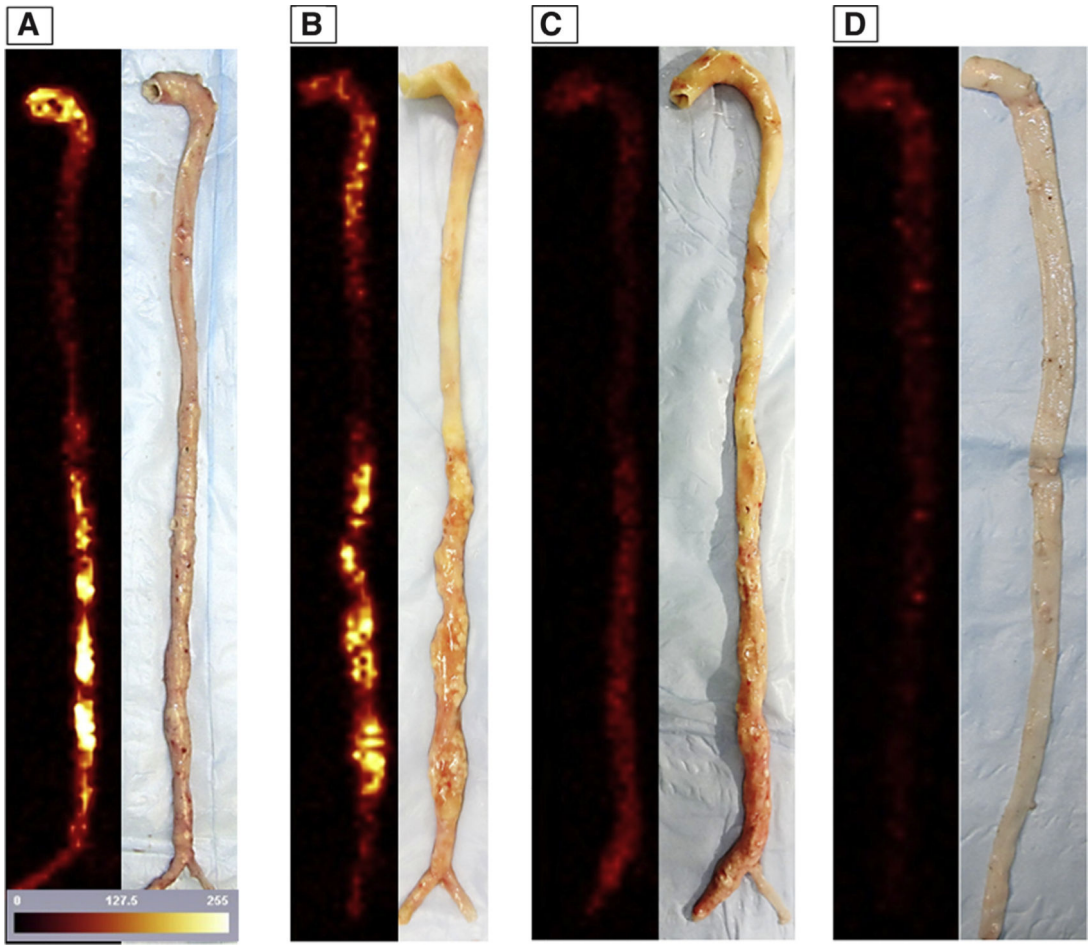

FIGURE 3. Harvested Aortas and Ex Vivo Images

Ex vivo images of the explanted aortas with ^{99m}Tc-duramycin (test tracer **[A]**) and ^{99m}Tc-annexin-V (positive control tracer **[B]**), compared with ^{99m}Tc-linear duramycin (negative radiotracer control **[C]**) for atherosclerotic animals, and ^{99m}Tc-duramycin (test tracer **[D]**) in disease control animal. Ex vivo images are adjacent to their corresponding gross picture. Please note that radiolabeled duramycin targeting is visually noninferior to annexin-V images.

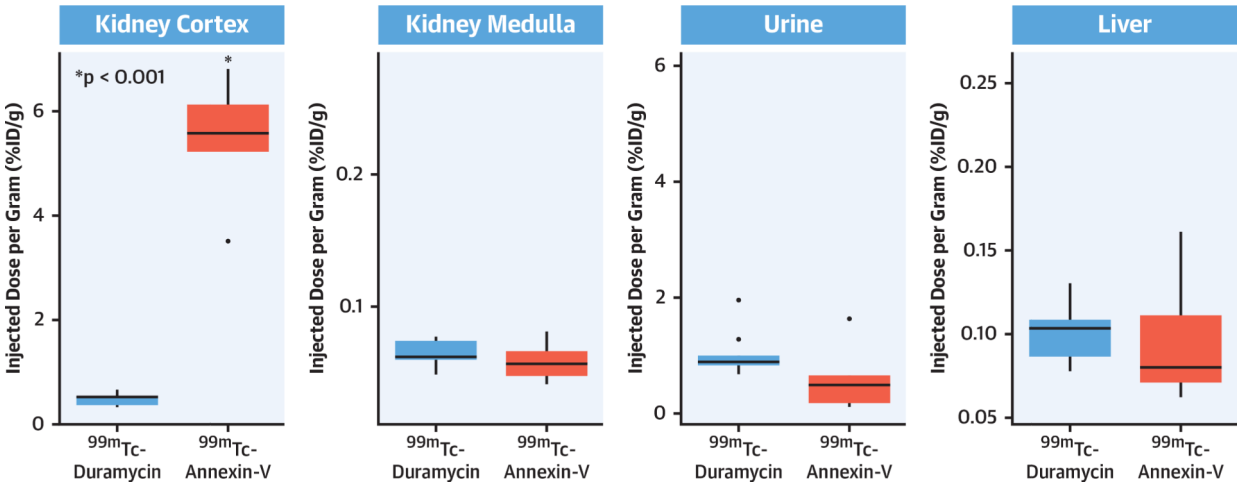

FIGURE 4. Radiation Burden for the Nontarget Organs

Quantitative %ID/g uptake in nontarget organs for ^{99m}Tc-labeled duramycin and annexin-V administered to atherosclerotic animals. Significant differences (*) are given in comparison with ^{99m}Tc-duramycin uptake. ID = injected dose.

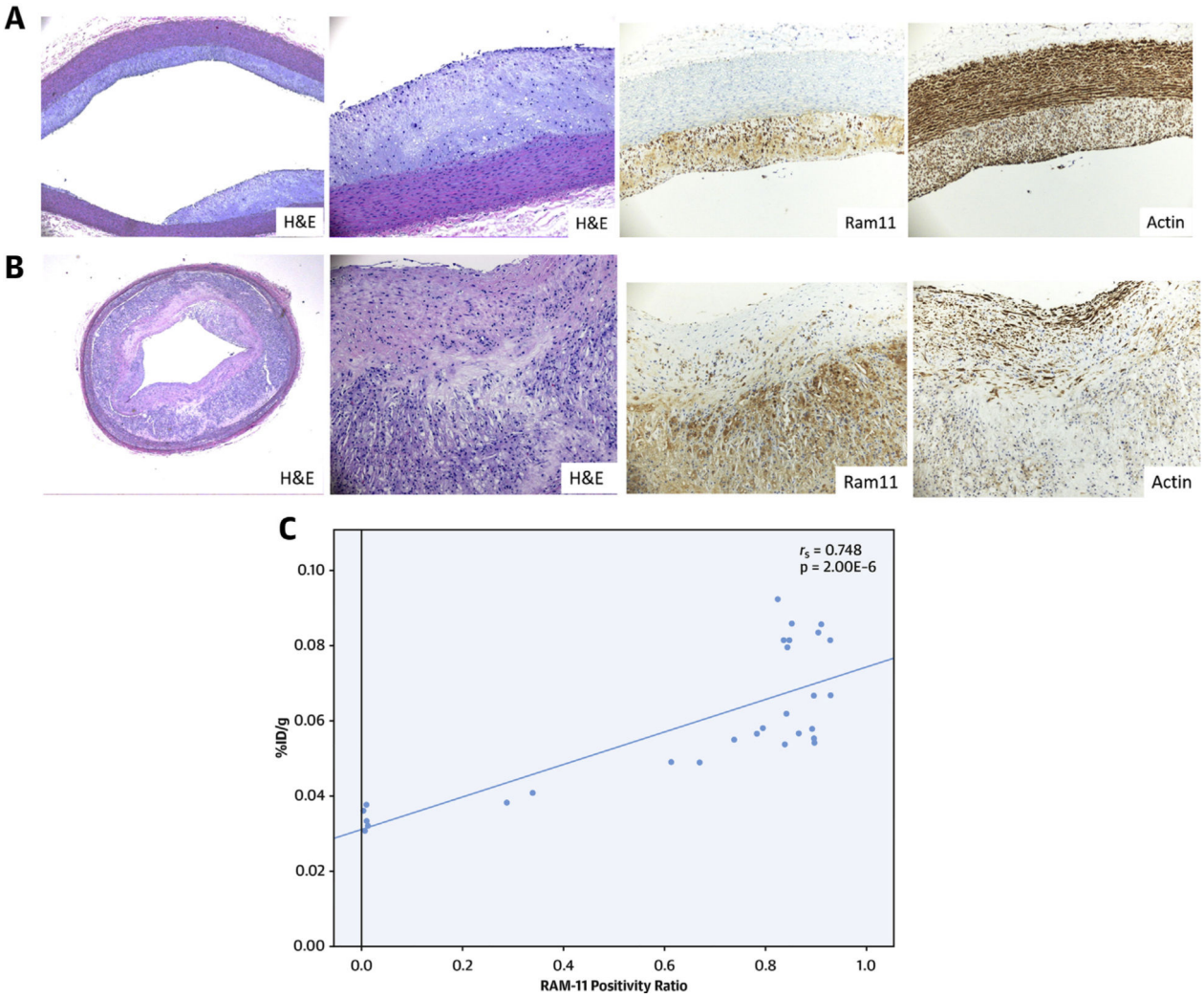

FIGURE 5. Histopathologic Characterization of Thoracic and Abdominal Aorta Samples

(A and B) Histopathological sections from the thoracic and abdominal aorta of a diseased animal, respectively. The **top rows** show low (x10) magnification, and the **bottom rows** show the microphotographs at high (×40) magnification. The **left 2 columns of both A and B** are stained with hematoxylin and eosin, whereas the **right 2 columns** are immunohistochemically stained with RAM-11 (macrophages, **column 3**) and HHF-35 (smooth-muscle cells, **column 4**). Pathological intimal thickening is seen in the thoracic region **(A)** compared with fibroatheromatous lesion **(B)** seen in the abdominal aorta. Staining is intense for the smooth-muscle cells in the medial layer and scattered in the neointima in the thoracic region **(A)**. Abundant inflammation is evident in the thick neointima carrying large necrotic core in the abdominal aorta specimen **(B)**. The duramycin uptake of the thoracic aorta segment was low at 0.002269 %ID/cm and 3-fold higher in the abdominal aorta segment of the same animal at 0.006824 %ID/cm. **(C)** The correlation of the RAM-11-stained aortic cross-sectional area with the respective piece-by-piece %ID/g uptake of 99mTc-duramycin. ID = injected dose.

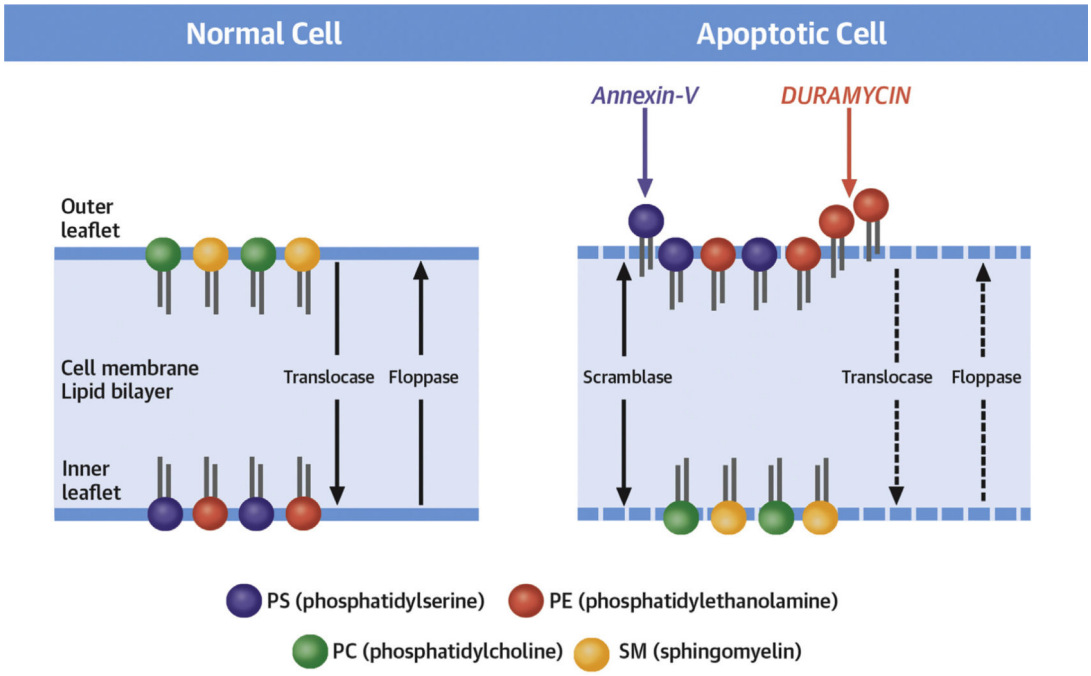

CENTRAL ILLUSTRATION. Molecular Imaging of Phospholipid Asymmetry During Apoptosis

The phospholipids in the cell membrane lipid bilayer are asymmetrically distributed with phosphatidylserine (PS) and phosphatidylethanolamine (PE) in the inner tab and phosphatidylcholine (PC) and sphingomyelin (SM) on the outer. This asymmetric distribution of phospholipids across the membrane bilayer is maintained by enzymes such as translocase and flippase. During apoptotic cell death, as a result of enzymatic alteration, normal phospholipid asymmetry within the cell membrane is lost, resulting in exteriorization of PS and PE. Activation of scrambalase exaggerates the random distribution. The exposure of PS acts as an “eat-me signal” for macrophages to have the apoptotic bodies removed. An endogenous protein, annexin-V possesses nanomolar affinity for externalized PS. Radiolabeled annexin-V has previously been used for noninvasive imaging of apoptotic cell death. Although effective for apoptosis imaging, annexin-V shows substantial off-target organ radiation burden. Like PS, apoptotic cell membranes also express PE. Even in larger quantities, PE can be targeted by an antibiotic-duramycin radiolabeled with technetium-99m. The current study compares the 2 probes targeted at the altered cell membranes. The study not only demonstrates the efficacy of imaging with duramycin but also its favorable off-target organ profile.